Langmuir

ARTICLE

pubs.acs.org/Langmuir

Detection of Interfacial Phenomena with Osteoblast-like Cell Adhesion on Hydroxyapatite and Oxidized Polystyrene by the Quartz Crystal Microbalance with Dissipation

Motohiro Tagaya,*[,†,‡] Toshiyuki Ikoma,[†,‡] Taro Takemura,[‡] Nobutaka Hanagata,[‡] Mitsuhiro Okuda,[‡] Tomohiko Yoshioka,[†] and Junzo Tanaka[†]

[†]Department of Metallurgy & Ceramics Science, Tokyo Institute of Technology, O-okayama 2-12-1, Meguro-ku, Tokyo 152-8550, Japan

[‡]Biomaterials Center, National Institute for Materials Science, Sengen 1-2-1, Tsukuba, Ibaraki 305-0047, Japan

Supporting Information

ABSTRACT: The adhesion process of osteoblast-like cells on hydroxyapatite (HAp) and oxidized polystyrene (PSox) was investigated using a quartz crystal microbalance with dissipation (QCM-D), confocal laser scanning microscope (CLSM), and atomic force microscope (AFM) techniques in order to clarify the interfacial phenomena between the surfaces and cells. The interfacial viscoelastic properties (shear viscosity (η_{ad}), elastic shear modulus (μ_{ad}), and tan δ) of the preadsorbed protein layer and the interface layer between the surfaces and cells were estimated using a Voigt-based viscoelastic model from the measured frequency (Δf) and dissipation shift (ΔD) curves. In the $\Delta D-\Delta f$ plots, the cell adhesion process on HAp was classified as (1) a mass increase only, (2) increases in both mass and ΔD, and (3) slight decreases in mass and ΔD. On PSox, only ΔD increases were observed, indicating that the adhesion behavior depended on the surface properties. The interfacial μ_{ad} value between the material surfaces and cells increased with the number of adherent cells, whereas η_{ad} and tanδ decreased slightly, irrespective of the surface. Thus, the interfacial layer changed the elasticity to viscosity with an increase in the number. The tan δ values on HAp were higher than those on PSox and exceeded 1.0. Furthermore, the pseudopod-like structures of the cells on HAp had periodic stripe patterns stained with a type I collagen antibody, whereas those on PSox had cell-membrane-like structures unstained with type I collagen. These results indicate that the interfacial layers on PSox and HAp exhibit elasticity and viscosity, respectively, indicating that the rearrangements of the extracellular matrix and cytoskeleton changes cause different cell−surface interactions. Therefore, the different cell adhesion process, interfacial viscoelasticity, and morphology depending on the surfaces were successfully monitored in situ and evaluated by the QCM-D technique combined with other techniques.

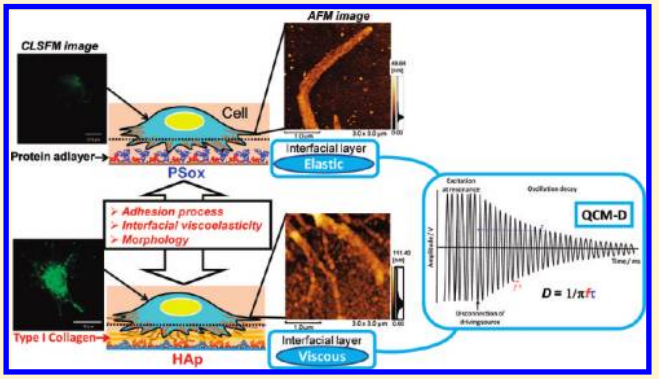

INTRODUCTION

Hydroxyapatite ($Ca_{10}(PO_4)_6(OH)_2$; HAp) is a biocompatible ceramic[1] and has been widely investigated with respect to its application in bone-filling materials with collagen[2−5] and as a drug-delivery carrier.[6−9] Its protein adsorption behavior is a critical issue and has been widely investigated.[10−12] The real-time adsorption of proteins on HAp nanolayer deposited with an electrophoretic deposition (EPD) method has also been investigated.[13−20] However, oxidized polystyrene (PSox) is a cytocompatible polymer[21] that is applicable in tissue culture dishes. The differences between HAp and PSox surfaces with respect to cell adhesion have not been elucidated, and there is little information on the interfacial phenomena between surfaces and cells. Thus, the interfacial phenomena with cell adhesion should be studied with the aim of designing superior biomaterial surfaces.

The cell adhesion behaviors depend on surface properties such as the topography, wettability, and charge and on the competitive and multiple adsorption of proteins.[22−24] The conformational change, denaturation, and arginine-glycine-asparagine (RGD) sequence of the proteins adsorbed on biomaterials directly govern the biocompatibility, which is attributed to the adhesion, proliferation, migration, and differentiation of cells.[25,26] An extracellular matrix (ECM) with the RGD sequence strongly affects cell adhesion.[27] Integrin binds to the RGD sequence in the ECM,[28] actin cytoskeletons are then produced, and the associated proteins form focal adhesion points at the surfaces.[29] The interfacial region close to the surface including

Received: January 3, 2011
Revised: May 6, 2011
Published: May 19, 2011

the binding of ECM−integrin−cytoskeleton affects the cell activities and functions. Thus, the in situ monitoring technique of the interface layers is of great importance.

The protein adsorption and subsequent osteoblast cell adhesion on the surfaces were previously reviewed by Aneslme.[24] The adsorption of different amounts of fetal bovine serum (FBS) on nanophase ceramics was found to cause different osteoblast cell adhesion.[30] In particular, HAp shows good biocompatibility with osteoblasts, and the features are attributed to the surface properties.[31−33] The proliferation and mineralization of osteoblasts on a HAp sintered body with and without preadsorbed type I collagen were investigated, revealing the various phenotype and gene expression patterns that were different from those on tissue culture polystyrene (TCPS).[34,35] If the cell behavior is determined by the adlayers of type I collagen, then the gene expression should be the same for the coatings of the type I collagen on HAp and TCPS. These results indicated that the cell functions were determined by the adsorption structure of the interfacial proteins. Therefore, it is indispensable to clarify the phenomena between the substrate surface adsorbed proteins and the cells during the initial adhesion stage.

Among the various means used to investigate the bimolecular interactions on the surfaces, the quartz crystal microbalance (QCM) was originally developed to measure mass changes at a gas−solid interface after Sauerbrey identified the linear relationship between a mass change for a piezoelectric substrate and a resonance frequency shift (Δf).[36] The development of suitable oscillator circuits made it possible to monitor adsorption behavior in organic liquids.[37] The cell viability and response to certain agents were first monitored with a piezoelectric sensor developed by Ebersole et al.[38] The QCM can detect the adhesion and spreading of cells[39,40] and is applicable to the cell−microparticle interaction.[41]

Various physical parameters with cell adhesion and spreading were measured to evaluate the viscoelastic properties of the cell layer, such as the resistance,[42−48] transient decay time by maximal oscillation amplitude,[51] and impedance.[49,50] Kasemo et al. suggested a quartz crystal microbalance with dissipation (QCM-D) technique for the in situ monitoring of the energy dissipation process with bimolecular adsorption,[52−62] which provides a rapid evaluation of the mass and viscoelasticity of the hydrated bimolecular adlayers. The QCM-D technique allowed the monitoring of the cell adhesion and spreading behaviors on PSox,[56−58,60,61] tantalum (Ta),[59−61] chromium (Cr),[59] titanium (Ti), and steel.[62] The QCM-D technique has also been used to understand the effect of the preadsorption of proteins on cell adhesion,[59−62] for example, on Ta and Cr with and without the preadsorption of FBS[59] and on Ti, TiO_2, and steel with the preadsorption of fibronectin or fibrinogen.[62] These results indicated that the preadsorption of the ECM proteins accelerates cell adhesion. However, the real-time in situ monitoring of cell adhesion on HAp as compared to that on other surfaces has not been investigated in detail. The interfacial viscoelastic property between HAp and cell adhesion should be investigated using the QCM-D technique.

In this study, the QCM-D technique was employed to characterize in situ osteoblast adhesion and spreading on PSox and HAp preadsorbed FBS proteins in order to provide further insight into the interfacial cell−surface interactions related to the cellular pseudopod-like structures. The interfacial viscoelastic parameters between the material surfaces and adherent cells were also calculated on the basis of a Voigt-based viscoelastic model. The morphology of the adherent cells was observed using atomic force microscope (AFM), confocal laser scanning microscope (CLSM), and confocal laser scanning fluorescence microscope (CLSFM) techniques. The different cell adhesion process, interfacial viscoelasticity, and morphology depending on the surfaces were evaluated to clarify the interfacial phenomena between the cells and surfaces.

EXPERIMENTAL SECTION

Materials. A gold sensor (QSX-301) and a PS sensor (QSX-305, film thickness of 40 nm on the gold sensor) were purchased from Q-Sense Inc. FBS (product number 12603C, lot no. 6D0975, SAFC Bioscience Co., Ltd.), alpha minimum essential medium (αMEM, Invitrogen Co., Ltd.) as a buffer for protein adsorption and cell adhesion, and phosphate-buffered saline (PBS, SEIMI Co., Ltd.) as a rinse solution were used. Ethanol (99.5 vol %), H_2O_2 (30 vol %), NH_3 (25 vol %), formaldehyde (37 vol %, special grade), t-butyl alcohol (99 vol %, special grade), and bovine serum albumin (BSA, 011-17844, biochemical grade) were supplied from Wako Chemical Co., Ltd. RBS@pF solution (<5% NaOH) as a detergent for the PS sensor was purchased from Sigma-Aldrich. Osteoblast-like MC3T3-E1 cells (RCB1126) as a cell line were provided by Riken BioResource Center. Trypsin (0.5%)-1 mM ethylenediaminetetraacetate (trypsin-EDTA, no. 25300) was purchased from Invitrogen. A plastic cell culture flask with an area of 75 cm^2 was purchased from BD Bioscience. A polyclonal rabbit antimouse collagen type I α2 chain (sc-28654) and fluorescein isothiocyanate-labeled goat antirabbit immunoglobulin G antibody (FITC-labeled IgG, F2765) were purchased from Santa Cruz Biotechnology and Invitrogen (VSA), respectively. All chemicals were used without further purification.

Preparation of PSox and HAp Sensors. The gold sensor was cleaned by immersing it into a 5:1:1 mixture of Milli-Q ultrapure water, H_2O_2, and NH_3 at 70 °C for 10 min. The PS sensor was cleaned with 10 vol % RBS@pF solution, Milli-Q ultrapure water, and ethanol. The sensors were then dried under N_2 gas flow and treated with UV light (λ = 254 and 185 nm, UV/ozone, Bioforce Nanoscience Co.) for 10 min in air. The PSox sensor and cleaned gold sensors were obtained.

The HAp nanocrystal was synthesized at 21 °C by a wet chemical method.[17] The HAp suspension was centrifuged at 2000*g* for 15 min, washed three times with ethanol, and ultrasonically dispersed in ethanol at 1 wt %. The HAp sensor was fabricated by the electrophoretic deposition (EPD) method reported in previous studies.[13,16] The cleaned gold sensor was used as an electrode, and a direct current voltage of 100 V/cm was applied for 1 min. The surplus nanocrystals were removed by ultrasonic treatment (28 kHz, 100 W) for 1 min in ethanol. To measure the film thickness, the HAp/gold patterns were fabricated by the partial masking on the gold before the EPD. The deposited weight of the HAp nanocrystals was measured in air using the QCM-D technique.

Cell Culture and Fabrication of Cell Suspension. Osteoblast-like cells were cultured in a cell culture flask containing 15 mL of FBS dispersed into αMEM at 10 vol % (10% FBS/αMEM). The cells were incubated at 37 °C in a humidified atmosphere of 5% CO_2 and subcultured every 7 days with 1 mL of trypsin-EDTA. After being washed with 15 mL of PBS and treated with 1 mL of trypsin-EDTA for 10 min at 37 °C, the cells were dispersed in 15 mL of PBS, separated by centrifugation (2000 rpm, 2 min), and dispersed in 15 mL of 10% FBS/αMEM. The centrifugation and dispersion were carried out twice. The number of cells in the suspension was counted and adjusted at seeding densities of 1.0×10^4, 2.5×10^4, 5.0×10^4, and 1.0×10^5 cells·mL^{-1}.

Real-Time Monitoring of FBS Adsorption and Cell Adhesion with the QCM-D Technique. QCM-D (D300, Q-Sense AB) measurement was performed at 37.0 ± 0.05 °C by monitoring Δf (Hz) and ΔD at 15 MHz. Δf was divided by the harmonic overtone number (n = 3) to obtain the value at the fundamental frequency of 5 MHz.

The monitoring of the preadsorption of FBS and the subsequent cell adhesion were conducted as follows. αMEM was introduced into the sample chamber to stabilize a baseline for 30−60 min, and then 10% FBS/αMEM was introduced at 0.5 mL and measured for 60 min. Subsequently, 0.5 mL of the suspended cells in 10% FBS/αMEM were seeded onto the FBS adlayers on PSox or HAp at seeding densities of 1.0×10^3, 2.5×10^3, 5.0×10^3, and 1.0×10^4 cells·cm^{-2}, cultured for 2 h in air, and finally rinsed with 0.5 mL of αMEM. Cell adhesion without the preadsorption of FBS was also conducted by the initial stabilization by αMEM and the subsequent injection of 0.5 mL of the cells dispersed into 10% FBS/αMEM at a concentration of 1×10^4 cells/cm^{-2}, with incubation for 2 h. The $\Delta D/\Delta f$ value of the adlayers was evaluated from the $\Delta D-\Delta f$ plots.[13]

The cells cultured on the sensors were removed from the sample chamber and then fixed with 3.7 vol % formaldehyde in PBS for 10 min at room temperature. The cells were washed two times with 1 mL of PBS before and after formaldehyde fixation. After the fixation, the cultured cells were soaked in a series of baths comprising 1 mL of EtOH/ultrapure water mixtures at 50, 60, 70, 80, 90, and 100 vol % with a soaking time of 5 min in each bath. The supernatant was then exchanged three times with t-butyl alcohol at 37 °C for 30 min per time, kept at 4 °C for 30 min, and finally freeze dried at 4 °C for 4 to 5 h.

The QCM-D data were simulated using the Q-tools software. Voinova et al. reported that the measured Δf and ΔD curves by the QCM-D technique have been fitted with a Voigt-based viscoelastic model to characterize the viscoelastic properties of the adlayers.[54,63] The viscoelastic property is represented by a complex shear modulus G^* given by eq 1.

$$G^* = G' + \mathrm{i}G'' = \mu_{\mathrm{ad}} + \mathrm{i}2\pi f\eta_{\mathrm{ad}} \tag{1}$$

where G' is the real part of G^*, G'' is the imaginary part of G^*, f is the oscillation frequency, μ_{ad} is the elastic shear modulus, and η_{ad} is the shear viscosity. The Δf and ΔD curves were monitored at 15 MHz and fitted with the Voigt-based viscoelastic model represented by the β function as follows.

$$\Delta f = \frac{Im(\beta)}{2\pi t_{\mathrm{q}}\rho_{\mathrm{q}}} \tag{2}$$

$$\Delta D = -\frac{Re(\beta)}{\pi f t_{\mathrm{q}}\rho_{\mathrm{q}}} \tag{3}$$

where β is represented by eq 4 with α, ξ_1, μ_{ad}, η_{ad}, d_{ad}, and ξ_2 and ξ_1 is represented by eq 5 with μ_{ad}, η_{ad}, and ρ_{ad} as follows.

$$\beta = \xi_1\frac{2\pi f\eta_{\mathrm{ad}} - \mathrm{i}\mu_{\mathrm{ad}}}{2\pi f}\frac{1-\alpha\exp(2\xi_1 d_{\mathrm{ad}})}{1+\alpha\exp(2\xi_1 d_{\mathrm{ad}})} \tag{4}$$

$$\xi_1 = \sqrt{-\frac{(2\pi f)^2\rho_{\mathrm{ad}}}{\mu_{\mathrm{ad}} + \mathrm{i}2\pi\eta_{\mathrm{ad}}}} \tag{5}$$

where α is represented by eq 6 with ξ_1, ξ_2, μ_{ad}, η_{ad}, and η_{l} and ξ_2 is represented by eq 7 with ρ_{l} and η_{l}, as follows.

$$\alpha = \frac{\frac{\xi_1}{\xi_2}\frac{2\pi f\eta_{\mathrm{ad}} - \mathrm{i}\mu_{\mathrm{ad}}}{2\pi f\eta_{\mathrm{l}}} + 1}{\frac{\xi_1}{\xi_2}\frac{2\pi f\eta_{\mathrm{ad}} - \mathrm{i}\mu_{\mathrm{ad}}}{2\pi f\eta_{\mathrm{l}}} - 1} \tag{6}$$

$$\xi_2 = \sqrt{\mathrm{i}\frac{2\pi f\rho_{\mathrm{l}}}{\eta_{\mathrm{l}}}} \tag{7}$$

where viscoelastic parameters such as μ_{ad}, η_{ad}, density (ρ_{ad}), and thickness (d_{ad}) were determined by using the density (ρ_{l}) and viscosity (η_{l}) of the bulk liquid. A one-adlayer model was applied to the data fitting with the Δf and ΔD curves of the FBS adsorption or cell adhesion because only the adsorption or adhesion was detected after the complete equilibrium of the ion from αMEM or FBS adsorption, respectively. In the case of FBS adlayers, the values of ρ_{l} and η_{l} were fixed at 1.000 g·cm^{-3} and 1.000 mPa·s, respectively, and ρ_{ad} was kept constant at 1.010−1.030 g·cm^{-3}.[65] The ρ_{l}, η_{l}, and ρ_{ad} values of the adherent cell layers were fixed at 0.993 g·cm^{-3}, 0.692 mPa·s, and 1.050 g·cm^{-3}, respectively.[49] The other parameters were optimized within the following boundaries: $\mu_{\mathrm{ad}} = 1 \times 10^2 - 1 \times 10^6$ Pa, $\eta_{\mathrm{ad}} = 0.692 - 100$ mPa·s, and $d_{\mathrm{ad}} = 1 \times 10^{-9} - 1 \times 10^{-5}$ m. The ratio of G'' to G' from eq 1 can be calculated as a loss tangent delta (G''/G') to evaluate the viscoelasticity of the adlayer as shown in eq 8.

$$\tan\delta = \frac{G''}{G'} \tag{8}$$

Characterization of Surfaces and Cells. The wettability of the sensor surfaces was analyzed in air by a sessile drop method using distilled water with a contact angle meter (CA-W200, Kyowa Interface Science Inc.). The droplet volume was 1.5 μL, and the area attached to the surfaces was 1.6 mm^2. The morphology of the cells was observed with a confocal laser scanning microscope (CLSM, OLS-3000, Olympus). The number of adherent cells on the sensors was counted over 20 different 1 mm^2 areas, and the spreading areas for the cells were measured for 50 cells in the 2D images. Three-dimensional images of the cells were acquired in 20−50 horizontal sections from cell tops to bottoms in the vertical direction to calculate the height and volume of the cells (n = 10). The structures of the surfaces before and after cell adhesion were observed with an atomic force microscope (AFM, SPM-9500, Shimazu). The surface roughness was calculated by the rms in the z-range images. A silicon nitride probe mounted on a cantilever (OMCL-AC160TS, Olympus) was employed in dynamic mode.

Immunostain of Type I Collagen for Osteoblast-like Cells on PSox and HAp. The cells cultured for 120 min were fixed with the same procedure as mentioned above and were stained at room temperature with 100 μL of the polyclonal rabbit antimouse collagen type I α2 chain as a primary antibody, which was diluted 15-fold in PBS including 1 wt % BSA for 4 h and washed three times with 1 mL of PBS. The samples were then incubated in the dark for 60 min with 100 μL of FITC-labeled IgG as a secondary antibody, which was diluted 15-fold in PBS including 1 wt % BSA and washed three times with 1 mL of PBS. The cells in PBS were covered and sealed with a glass to prevent evaporation during the observation with a confocal laser scanning fluorescence microscope (CLSFM, TCS SP-5, Leica Microsystems).

RESULTS AND DISCUSSION

Preadsorption of FBS on Sensors. Figure 1 shows AFM topographic images of PSox and HAp surfaces over an area of 1 × 1 μm^2. The PSox and HAp surfaces deposited on the bare gold surface had rms values of 0.4 ± 0.2 and 4.4 ± 0.4 nm, respectively, which were almost the same as that of gold with a value of 0.8 ± 0.4 nm. The weight change of the HAp nanocrystals on gold with the EPD was 4.0 ± 0.2 μg·cm^{-2}, and the thickness of the nanolayer was estimated to be 10−20 nm (based on a density of HAp of 3.14 g·cm^{-3}), which corresponds to the previous report[13] and the AFM height line profile between the gold and HAp nanocrystal surfaces (Supporting Information, Figure S1). The phase-shift images of the HAp surfaces have a uniform brightness (data not shown), indicating the homogeneous deposition of HAp nanocrystals. PSox and HAp are hydrophilic surfaces with contact angles for water of 34.6 ± 4.1 and 48.7 ± 2.1°, respectively. Thus, PSox and

dx.doi.org/10.1021/la200008z |Langmuir 2011, 27, 7635–7644

HAp sensor surfaces with a flat surface a few nanometers away were successfully fabricated.

Figure 2 shows the Δf and ΔD curves and $\Delta D-\Delta f$ plots of FBS adsorption on PSox and HAp. The curves indicate that the adsorption reached a plateau at 20 min on PSox and at 15 min on HAp. The Δf and ΔD curves indicate the adsorption equilibrium states at 60 min. The Δf and ΔD values at 60 min were -59.5 ± 3.5 Hz and $(+4.9 \pm 1.8) \times 10^{-6}$ on PSox and -44.9 ± 4.0 Hz and $(+1.2 \pm 0.6) \times 10^{-6}$ on HAp, and the saturated $\Delta D/\Delta f$ values of the FBS adlayers were $(-8.3 \pm 1.7) \times 10^{-8}$ 1/Hz on PSox and $(-4.1 \pm 1.6) \times 10^{-8}$ 1/Hz on HAp. The adsorbed amount and absolute $\Delta D/\Delta f$ value of the FBS adlayer on HAp were smaller than those on PSox. We previously reported that the slight adsorption of carbonate ions from αMEM on HAp caused a decrease in the adsorbed amount of FBS and the degradation of the viscoelastic property of the FBS adlayer.[18,19] PSox would suppress the adsorption of carbonate ions to show larger values.

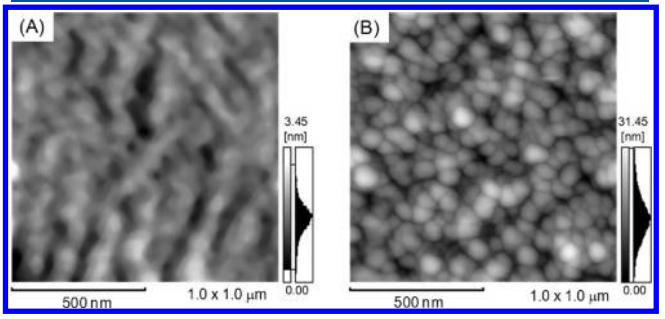

Figure 1. AFM topographic images of (A) PSox and (B) HAp over an area of $1 \times 1\ \mu m^2$.

The thin films of HAp and PSox tightly adhered to the gold, and the visicosity effect due to the flexibility of the film is vanishingly small. Therefore, the difference in the protein adsorption behavior was attributed to the surface properties of the sensor.

On the basis of the Voigt-based viscoelastic model, the viscoelastic parameters of the FBS adlayer on PSox were determined to be $\mu_{ad} = 33.41 \pm 5.52$ kPa, $\eta_{ad} = 1.76 \pm 0.26$ mPa·s, $\rho_{ad} = 1.02 \pm 0.01$ g·cm^{-3}, and $d_{ad} = 19.2 \pm 5.7$ nm, whereas those on HAp were $\mu_{ad} = 89.44 \pm 7.28$ kPa, $\eta_{ad} = 2.09 \pm 0.09$ mPa·s, $\rho_{ad} = 1.04 \pm 0.02$ g·cm^{-3}, and $d_{ad} = 22.0 \pm 0.6$ nm. The μ_{ad} and η_{ad} values for HAp were higher than those for PSox, whereas the ρ_{ad} and d_{ad} values were irrespective of the surface. The tan δ value of 0.74 ± 0.40 for HAp was lower than that of 1.73 ± 0.52 for PSox. The results indicate the viscous adlayer on HAp as compared with that on PSox. It is speculated that the multiple proteins in FBS competitively adsorb on the surfaces and the adsorbed species and structures depend on the surface properties. The viscoelastic parameters of the FBS adlayer on the surfaces were very similar to those of the albumin adlayer on gold, which had $\mu_{ad} = 100$ kPa, $\eta_{ad} = 6$ mPa·s, and tan $\delta = 1.8$,[64] whereas those of the laminin adlayer on gold were $\mu_{ad} = 7.6 \pm 1.9$ kPa, $\eta_{ad} = 1.83 \pm 0.11$ mPa·s, and tan $\delta = 7.6$.[65] The elastic property of the FBS adlayer on HAp compared to that on PSox corresponds to the tendency of the saturated absolute $\Delta D/\Delta f$ values. These different viscoelastic properties of the adlayers could affect the cell adhesion behavior.

In Situ Monitoring of the Adhesion Behavior of Osteoblast-like Cells. Figure 3 shows the $\Delta D-\Delta f$ plots of the adhesion behaviors of the cells on PSox and HAp for 120 min, and expanded plots of the saturated regions at a seeding density of 1.0×10^4 cells·cm^{-2} are shown in the insets. Here, the

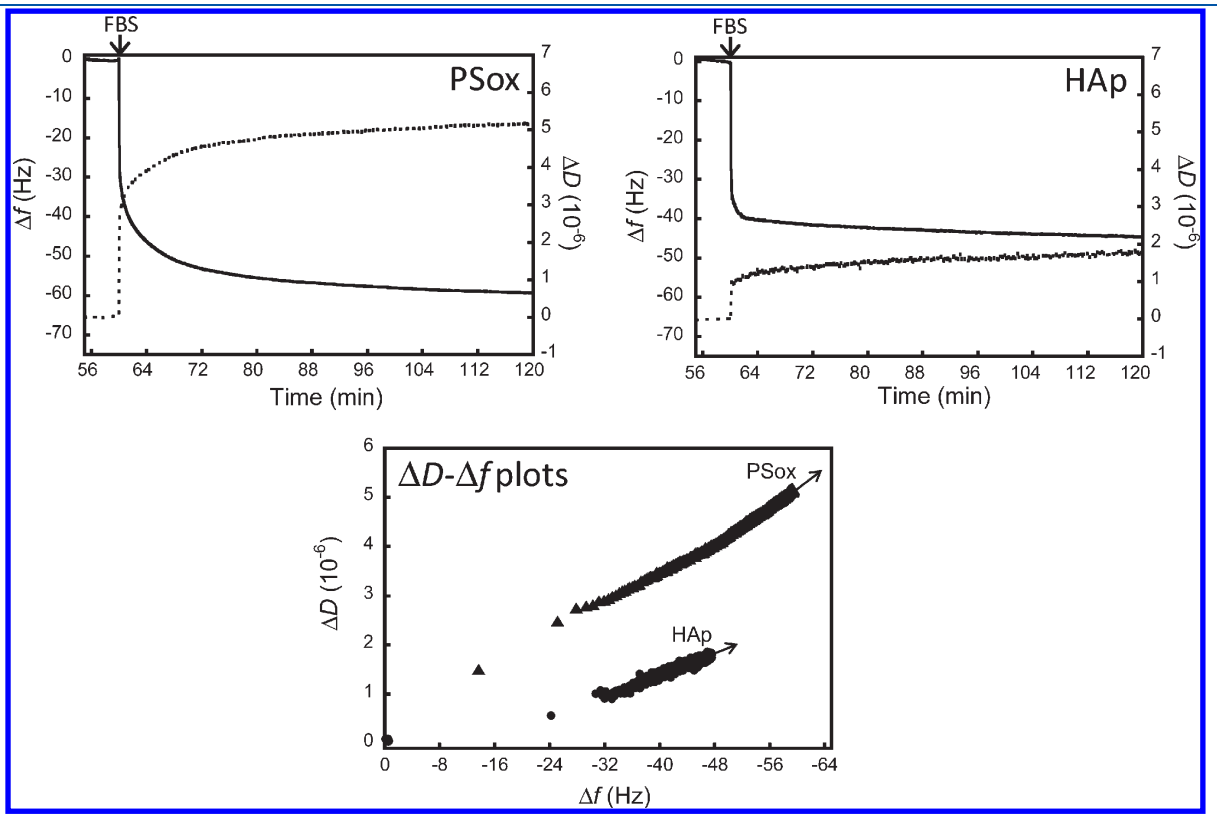

Figure 2. Δf and ΔD curves and $\Delta D-\Delta f$ plots of FBS preadsorption on PSox and HAp. Δf was transformed into the value for the fundamental frequency of 5 MHz by dividing by 3, which was the harmonic overtone number.

dx.doi.org/10.1021/la200008z |*Langmuir* 2011, 27, 7635–7644

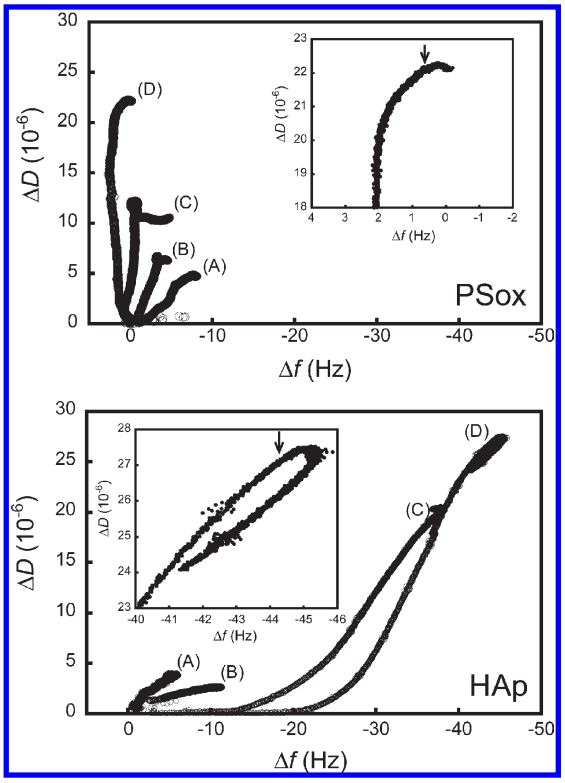

Figure 3. $\Delta D-\Delta f$ plots of the osteoblast-like cells adhered on PSox and HAp for 2 h. The seeding densities were (A) 1.0×10^3, (B) 2.5×10^3, (C) 5.0×10^3, and (D) 1.0×10^4 cells·cm^{-2}. The insets show the expanded plots of the cells at 1.0×10^4 cells·cm^{-2}. The arrows indicate the point at 1 h. The Δf values were transformed into values for the fundamental frequency of 5 MHz by dividing by 3, which was the harmonic overtone number.

injection of the cell suspension after the equilibrium state of FBS adsorption would induce the reaction of the cells with the preadsorbed FBS surfaces. The adhesion behavior of the cells on PSox was different from that on HAp, which also depended on the seeding density. The Δf and ΔD curves at 1.0×10^3 cells·cm^{-2} showed very similar tendencies on both PSox and HAp with a decrease in Δf (i.e., an increase in mass) and with an increase in ΔD (Supporting Information, Figure S2). However, the $\Delta D-\Delta f$ plots for PSox and HAp surfaces without the preadsorpiton of FBS at a seeding density of 1.0×10^4 cells·cm^{-2} (Supporting Information, Figure S3) indicated little mass and ΔD increases with cell adhesion, taking into account the fast kinetics of protein adsorption as compared with that of cell adhesion,[72] indicating the significant interfacial protein effect on cell adhesion. These results clearly suggested that the cell adhesion and spreading processes occurred on the interfacial protein adlayers on the surfaces.

Interestingly, little mass increase on PSox was detected during the cell adhesion process, with only an increase in ΔD measured at 5.0×10^3 and 1.0×10^4 cells·cm^{-2}. The $\Delta D-\Delta f$ plots for PSox at 5.0×10^3 and 1.0×10^4 cells·cm^{-2} clearly showed the characteristic adhesion behaviors, which were classified into two regions: (I) an increase in ΔD for 60 min and (II) a slight increase in mass with a slight decrease in ΔD for 60−120 min. This tendency corresponds to that of the fibroblast adhesion on the fibronectin-preadsorbed PSox and on the FBS-preadsorbed Ta,[60,61] and the f and D changes were due to the morphological changes followed by the extracellular matrix remodeling as well as cytoskeletal changes. In this study, region I reflects the morphological changes in the cells upon approach, and region II reflects the increase in the surface coverage of the cells upon adhering and spreading.

The adhesion process of the cells on HAp depended on the seeding density. An increase in the seeding density caused an increase in mass and a subsequent increase in ΔD. The $\Delta D-\Delta f$ plots for HAp at 5.0×10^3 and 1.0×10^4 cells·cm^{-2} were clearly classified into three regions: (I) an increase in just the mass for 5 min, (II) an increase in both the mass and ΔD for 5−60 min, and (III) an decrease in both the mass and ΔD for 60−120 min. The Δf values on HAp were clearly larger as compared with those on PSox, indicating the tight protein−cell interactions on HAp. The initial Δf decrease was related to an increase in the number of adherent cells.[60] Region I would reflect the approach of the cells to HAp. Once the cells approach the surface, they quickly remodel the adsorbed proteins to suit their requirements and interact with the ECM proteins on the surface.[60,61,66] Thus, region II would predominately indicate the protein remodeling and a cellular morphological change, and region III would indicate a change in the plasma membrane rigidity through the ECM−integrin−cytoskeleton at the interface. Therefore, the QCM-D technique was successfully used for in situ real-time monitoring of the different cell adhesion processes depending on the substrate surfaces.

Table 1 lists the Δf and ΔD values, numbers, and areas of the cells adhering to PSox and HAp at 2 h. The areas, heights, and volumes of the cells adhering to PSox and HAp showed no differences in statistical errors, and these values are almost the same irrespective of the seeding density. The number of adherent cells on both surfaces was found to increase linearly against the seeding density with different slopes after being fitted with a simple equation. The number of adherent cells on PSox was larger than that on HAp below 5×10^3 cells·cm^{-2} and became smaller at 1×10^4 cells·cm^{-2}. The seeding density strongly affected the cell adhesion rate on PSox, with values of over 70% for 1.0×10^3 cells·cm^{-2}, and gradually decreased to approximately 30%. The cell adhesion rates on HAp increased with the seeding density, with values of 25% at 1.0×10^3 cells·cm^{-2} and 50% at 1×10^4 cells·cm^{-2}. The Δf change against the number of adherent cells on PSox showed a positive nonlinear relationship, meaning that the mass decreased with the seeding density, but the ΔD values showed a linear correlation. The Δf changes on HAp almost linearly increased below 5×10^3 cells·cm^{-2} and reached a plateau at 1×10^4 cells·cm^{-2}. The general seeding density of the osteoblast-like cells in culture is well known to be 1.0×10^3−2.0×10^3 cells·cm^{-2}, which is the monodispersion state of the adhered cells in the initial stage. Thus, the nonlinearity at 1×10^4 cells·cm^{-2} would be attributed to the influence of neighboring cells.

Viscoelastic Property of Interface Layers between the Sensor Surfaces and the Adherent Cells. The difficulty in interpreting the cell adhesion behavior is attributed to the theoretical differences in the soft mass loading on the surface, which cannot behave like the rigid mass model proposed by Sauerbrey.[36] Wegener et al. showed that the adhesion of different cell lines on gold caused different time course curves for Δf and different apparent viscosities (η_{app}).[49] The η_{app} values were calculated by measuring the viscosities of glycerol−water systems using a Gordon−Kanazawa equation[67] and were determined to be 1.86 ± 0.08 mPa·s for MDCK-II, 1.29 ± 0.05 mPa·s for MDCK-I, and 1.12 ± 0.04 mPa·s for fibroblast 3T3 on the basis of a cell density of 1.05 g·cm^{-3}. Furthermore, the rat osteoblast-like

dx.doi.org/10.1021/la200008z |Langmuir 2011, 27, 7635–7644

Table 1. Frequency Shift (Δf), Dissipation Shift (ΔD), Number of Adherent Cells, and Area of the Cells Adhered on PSox and HAp at 120 min against the Seeding Density

	Δf (Hz)	ΔD ($\times 10^{-6}$)	number of adherent cells (cells·cm^{-2})	area (μm^2·cell^{-1})
PSox (1.0×10^3 cells·cm^{-2})	-9.3 ± 1.7	$+3.7 \pm 1.4$	730 ± 150	2270 ± 590
PSox (2.5×10^3 cells·cm^{-2})	-4.5 ± 0.8	$+6.3 \pm 1.4$	960 ± 220	1990 ± 680
PSox (5.0×10^3 cells·cm^{-2})	-4.8 ± 0.5	$+10.5 \pm 1.8$	2160 ± 260	1740 ± 640
PSox (1.0×10^4 cells·cm^{-2})	-0.1 ± 0.1	$+22.1 \pm 5.5$	3400 ± 410	1650 ± 790
HAp (1.0×10^3 cells·cm^{-2})	-5.9 ± 0.1	$+3.8 \pm 1.2$	250 ± 130	1500 ± 500
HAp (2.5×10^3 cells·cm^{-2})	-11.1 ± 0.7	$+2.6 \pm 0.7$	590 ± 220	1960 ± 610
HAp (5.0×10^3 cells·cm^{-2})	-36.9 ± 2.3	$+20.3 \pm 3.5$	2150 ± 190	1320 ± 300
HAp (1.0×10^4 cells·cm^{-2})	-41.3 ± 2.9	$+24.1 \pm 4.8$	4980 ± 190	1900 ± 500

cells had an η_{app} of 3 mPa·s.[68] The cell adhesion behavior, mainly Δf, was thus ascribed to the density−viscosity products of the confluent cell layers, which were mainly due to the cytoplasmic viscosities despite the presence of an aqueous or proteinaceous intermediate layer of cells and substrates. To apply this model to the present study, the η_{app} values were calculated to be 1.9×10^{-8} mPa·s on PSox and 3.4×10^{-3} mPa·s on HAp, which were extremely small as a result of the oscillator circuit model difference from the QCM-D system.

Only a few studies of the viscoelastic property of the protein adlayer based on the Voigt-based viscoelastic model have been conducted,[54,63] but the viscoelastic property of the interface between the material surface and the cell has not been reported. The adhesion behavior dependent on the surface is attributed to the cell−surface interactions at the interface. Thus, the evaluation of interfacial phenomena based on the Voigt-based model would be an effective tool. The model was applied in this study, and the results were obtained as shown in Figure 4, which shows the viscoelastic parameters of μ_{ad}, η_{ad}, and d_{ad} for PSox and HAp with the adherent cell number. With an increase in the seeding density, the μ_{ad} and d_{ad} values on the surfaces increased and the η_{ad} and tan δ values decreased. Thus, the adherent cell layers changed the elasticity to viscosity with an increase in the cell number, indicating the enhancement of cell−surface and cell−cell interactions. The μ_{ad} values on PSox were higher than those on HAp. The η_{ad} values for PSox and HAp were almost same, whereas the tan δ values for HAp were apparently larger than those for PSox. This indicated that the interfacial layer of the cells adhered on HAp had a certain viscosity compared to that on PSox. The d_{ad} values of the adherent cells on HAp (i.e., the average thickness of the interfacial layer of adherent cells) were higher than those on PSox, which also caused the viscosity on HAp. The Voigt mass of the adherent cell layers was calculated from the d_{ad} values, and the adlayer density of the cells was assumed to be 1.05 g·cm^{-3}. The Voigt mass of one cell on PSox remained almost the same at 1 to 2 ng·cell^{-1} for different seeding densities, whereas that on HAp decreased from 10 to 2 ng·cell^{-1} with an increase in the number of adherent cells. From these results, it is speculated that the adherent cells on HAp secreted visous, high-density substitutes such as ECM at the interfacial layer. Therefore, the Voigt-based model clearly reveals the interfacial viscoelastic properties that depend on the sensor surface.

In the QCM-D measurement, the detectable height (l) of the D value on the sensor surface was limited and is expressed as eq 9.

$$l = \left(\frac{\eta}{\pi\rho f}\right)^{1/2} \quad (9)$$

where η and ρ are the density and viscosity of the liquid, respectively, and f is the resonance frequency.[50,63] A higher η value for the adlayer can detect in a higher l region. The l of a resonating wave in water at 37 °C with ρ = 0.993 g/cm^3 and η = 0.692 mPa·s was calculated to be 110 nm at 15 MHz.[49] The FBS adlayer with the viscoelastic values measured in this study had an l of 190−210 nm at 15 MHz. The l of the adherent cell layers decreased from 200 to 120 nm at 15 MHz with an increase in the number of adherent cells; these values of l were much shorter than the actual height of cells, which was on the order of micrometers. This suggested that the QCM-D measured the lower parts of cells close to the FBS adlayer on the sensors. The viscoelastic parameters and d_{ad} values were within the detectable height of the D value using 15 MHz. The interfacial layer composed of the cell cytoskeletons, cell membranes, pseudopods, and protein adlayer on the sensor surfaces is approximately 10−200 nm according to a previous report,[73] which is consistent with the detectable l at 15 MHz. However, in the use of the higher harmonics at 25 and 35 MHz, l is much lower than in the region of the interfacial layer. Therefore, the QCM-D effectively measured the lower parts of the cells close to the sensor surfaces.

Li et al. described the viscoelastic properties of a fibroblast monolayer on a gold surface using a thickness shear mode quartz crystal resonator with a transfer matrix method.[71] They calculated μ_{ad} values of 21−39 kPa and η_{ad} values of 0.92−1.56 mPa·s at a 5 MHz resonance frequency, which are very similar to the results of the present study. The tan δ values of 1.2−2.3 were apparently smaller than our results, and the differences could be caused by the resonance frequency of the quartz crystal used. Fernández et al. investigated the viscoelastic properties of a fibroblast monolayer with a rheometer and obtained G', G'', and tan δ values at 10 Hz of 400 Pa, 150 Pa, and 0.3, respectively, indicating that the cell monolayer was an elastic body.[69] The viscoelastic parameters were different from our results, which would be attributed to the measured frequency or detectable height on the surface. Palmer et al. indicated that the elastic shear modulus dominates the viscoelastic property of the cells because of their rigid cytoskeletons at lower frequencies but that the viscous modulus dominates the property because of the cytoplasmic fluid at higher frequencies.[70] They suggested that the actin networks at a high frequency of 1 MHz would show a liquidlike property and those at a low frequency of 10 Hz would show an elastic property. In this study, the QCM's high frequency of 15 MHz caused the viscosity behavior of the adherent cells as a result of the dependence of the cytoskeleton property on the frequency. The different viscoelastic properties of the adherent cells on PSox and HAp could be attributed to the different cytoskeleton structures and cellular secretion of the ECM close

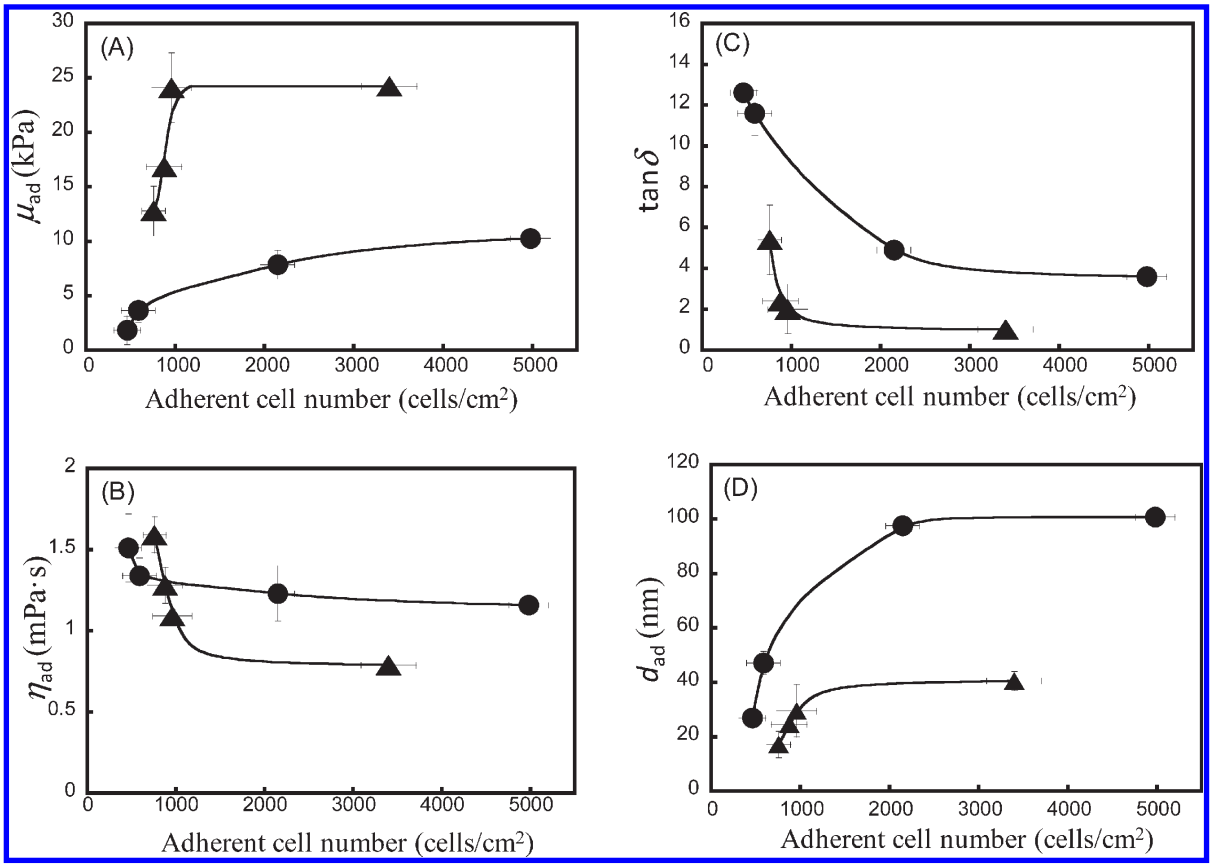

Figure 4. Plots of (A) elastic shear modulus (μ_{ad}), (B) shear viscosity (η_{ad}), (C) tan δ, and (D) thickness (d_{ad}) values of the interfacial layers of the cell on PSox (▲) and HAp (●) at 120 min against the seeding density.

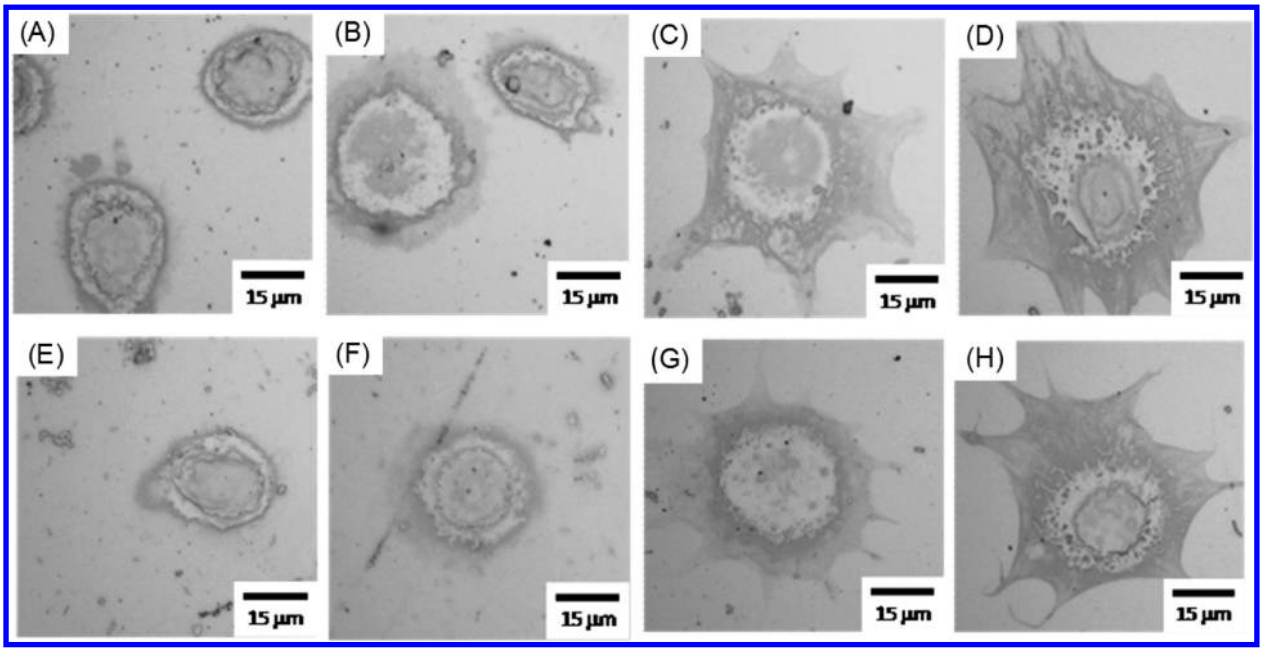

Figure 5. Light microscope images of the cells adhered to (A–D) PSox and (E–H) HAp, which were incubated for (A, E) 5, (B, F) 30, (C, G) 60, and (D, H) 120 min. The seeding density was 1.0×10^4 cells·cm^{-2}.

to the sensor surfaces. Therefore, the interface between the material surfaces and cells by the Voigt-based model successfully caused the differences in the interfacial viscoelastic properties depending on the surfaces.

dx.doi.org/10.1021/la200008z |*Langmuir* 2011, 27, 7635–7644

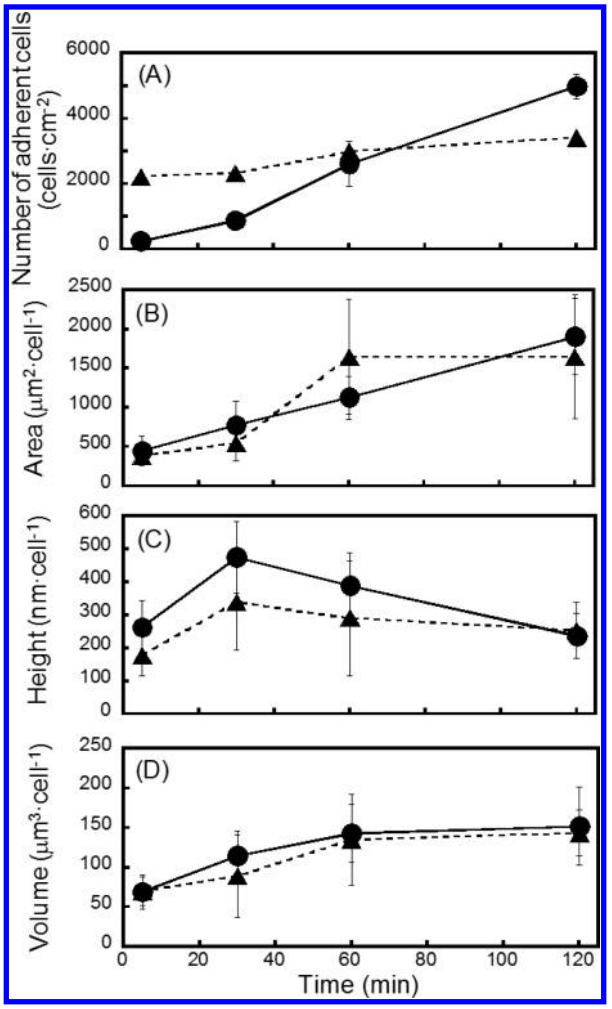

Figure 6. Time course curves for (A) the number of adherent cells, (B) the area, (C) the maximum height, and (D) the volume of cells adhered to PSox (▲) and HAp (●) at 1.0×10^4 cells·cm^{-2}.

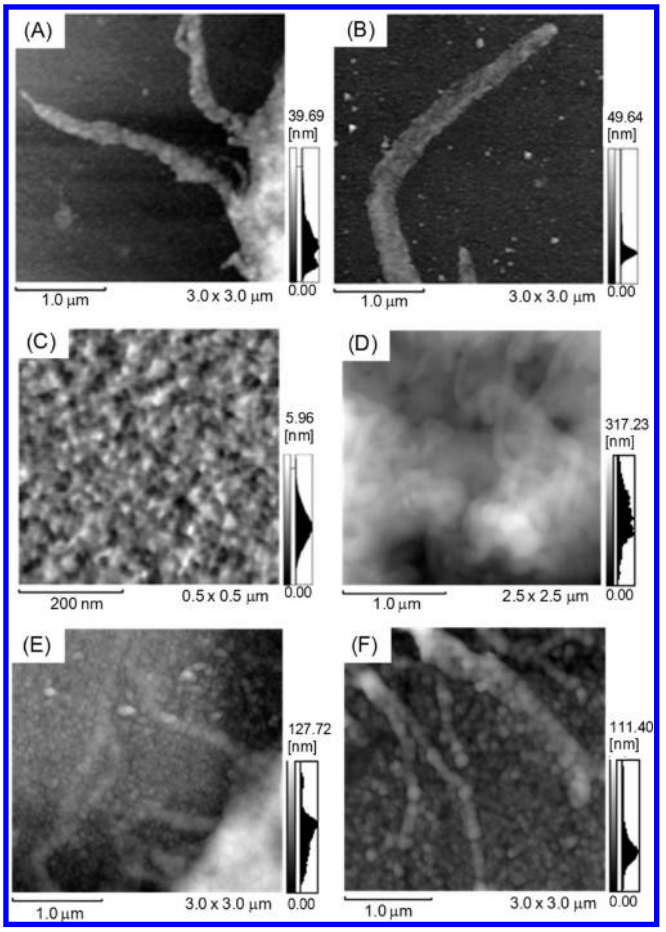

Figure 7. AFM topographic images of (A, B) the pseudopod-like structures of cells adhered on PSox and (C−F) the structures of cells on HAp: (C) the outer surfaces on the nuclei, (D) the surrounding outer surfaces around the nuclei, and (E, F) the pseudopods close to the sensor surfaces.

Microscopy Characterization of Adherent Cells. Figure 5 shows CLSM images of the osteoblast-like cells adhering to PSox and HAp. The morphologies of the cells were apparently changed, and the adhesive area was increased with the incubation time. The cells incubated at 5 and 30 min had a round shape with diameters of 18−25 μm at 5 min and 20−35 μm at 30 min, and the cells started spreading and formed pseudopods at 60 min, irrespective of the sensor surface. Different pseudopod-like structures for the cells were observed at 120 min, with planular pseudopods on PSox and cuspate and fibrous pseudopods on HAp. The average diameters and adhesive areas of the cells on PSox and HAp were similar at 60−70 μm and 1600−1800 μm^2, respectively, irrespective of the sensor surface. Modin et al. reported that the osteoblast-like cells on Ta and Cr had different adhesive areas, with a ratio of Ta to Cr of 66% under FBS-free conditions.[59] The average diameters on Ta and Cr were 100 μm smaller than those on PSox and HAp, suggesting that the difference in the substrate components affected the adhesion behaviors of the cells. The adherent cells on PSox and HAp surfaces without the preadsorpiton of FBS show average diameters and adhesive areas at 15−30 μm and 800−1000 μm^2 (809.0 ± 187.0 μm^2 for PSox and 1064.8 ± 257.0 μm^2 for HAp; Supporting Information, Figure S4) at 120 min, respectively, and are significantly smaller than those occurring with preadsorption, indicating that cell spreading clearly occurs on the FBS adlayers.

Figure 6 shows the changes in the numbers, areas, maximum heights, and volumes of the cells adhered to PSox and HAp against the incubation time at a seeding density of 1×10^4 cells·cm^{-2}. The cells rapidly adhered to PSox after 5 min of incubation, and the number of adherent cells was approximately 20%. Increasing the incubation time caused only a small increase in the number of adherent cells. In contrast, the number of adherent cells on HAp gradually increased with the incubation time, which could have affected the changes in the Δf and ΔD values in the QCM-D measurements. The number of adherent cells on the surfaces without the preadsorpiton of FBS is 1540 ± 320 cells·cm^{-2} for PSox and 1550 ± 240 cells·cm^{-2} for HAp at 120 min (Supporting Information, Figure S4); these values are much smaller than those occuring with preadsorption, indicating the importance of the preadsorption of FBS for cell adhesion. Although the data, with the exception of the number of adherent cells, were within the statistical errors, the area and volume of the cells adhering to the surfaces gradually increased and the height reached a maximum after 30 min of incubation time, particularly on HAp. It was found that the numbers and areas with the interfacial reaction between the proteins and cells clearly changed with time.

dx.doi.org/10.1021/la200008z |*Langmuir* 2011, 27, 7635–7644

Figure 7 shows AFM topographic images of the different parts of the cells incubated for 120 min on PSox and HAp. The cells on PSox formed thick pseudopods, as shown in Figure 7A; these pseudopods had dense particulate structures with no periodic stripes, as shown in Figure 7B. The pseudopods would be derived from the spread of cell membranes on PSox. The surface on the nuclei of cells on HAp showed a typical cell membrane structure that could be represented by a fluid mosaic model with an rms of 0.9 ± 0.5 nm over 0.5 × 0.5 μm^2, as shown in Figure 7C. As shown in Figure 7D, the surrounding surface on HAp had a rough fibrous structure with an rms of 52.3 ± 9.3 nm over 2.5 × 2.5 μm^2, which could reflect a cytoskeleton. Without the pseudopods, these surface structures of the cells in Figure 7C, D on PSox and HAp were very similar. Figure 7E,F show the cuspate and fibrous pseudopod-like structures on HAp, respectively. Interestingly, these pseudopods had a significant periodic stripe pattern with an interval of 60−70 nm similar to that of type I collagen fibrils from the height line profiles (Supporting Information, Figure S5). Furthermore, the average widths of these pseudopods on PSox and HAp were 275.8 ± 70.6 and 135.4 ± 49.5 nm, and those on HAp were smaller than those on PSox. The interfacial pseudopod structures are clearly different depending on the sensor surfaces. Thus, it is speculated that the pseudopods on PSox are part of the cell membrane whereas those on HAp are composed of both the cell membrane and the extracellular matrix produced by the cells. The different interfacial structures would affect the adhesion behaviors and interfacial viscoelastic properties.

The cells adhering to PSox and HAp after 120 min of incubation after staining were observed by FCLSM (Supporting Information, Figure S6). PSox- and HAp-adsorbed FBS exhibited no fluorescence signals from the whole region and were unstained. The cells on PSox exhibited weak fluorescence signals from the whole region, and the pseudopods were unstained by type I antimouse collagen. This indicated that the cells spreading on PSox could produce only a small amount of type I collagen. However, the cells on HAp were preferentially stained over the whole area; in particular, the fibrous pseudopods were stained with the type I antimouse collagen. This indicated that the fibrous pseudopods were composed of type I collagen produced by the cells; these results were almost coincident with that obtained by the AFM observation. The pseudopods on PSox are part of the cell membrane, whereas those on HAp are composed of both the cell membrane and cell-driven type I collagen. The interfacial structures affect the elastic and viscous layers on PSox and HAp, respectively. Therefore, the recognition of the cells on the surfaces caused different adhesion behavior and interfacial viscoelastic layers depending on the surfaces, which are successfully monitored and evaluated by QCM-D combined with other techniques.

CONCLUSIONS

QCM-D combined with other techniques (AFM, CLSM, and CLSFM) was used in situ to analyze the adhesion behavior of the osteoblast-like cells on PSox and HAp in order to clarify the interfacial phenomena between the surfaces and cells. From the $\Delta D-\Delta f$ plots, the cellular adhesion and spreading behaviors clearly depended on the differences between PSox- and HAp-surface preadsorbed FBS. The adhesion speed on PSox was more rapid than that on HAp, which could also have caused the difference in the $\Delta D-\Delta f$ plots, indicating that the preadsorbed FBS on the surfaces effectively governed the cell adhesion process. The viscoelastic property of each adherent cell layer was calculated using the Voigt-based model, and the interface between the surface and cell causes the differences in the viscoelasticities depending on the surface properties. The adherent cell layers on HAp exhibited viscosity as compared with those on PSox. The pseudopod structures adhering to PSox and HAp were apparently different: the pseudopods on PSox had a cell-membrane-like structure, and those on HAp were composed of the cell membrane and type I collagen produced by the cells. It is speculate that the adherent cells on PSox expanded the cytoskeletons without secreting type I collagen, whereas those on HAp clearly secreted type I collagen at the interface to show the viscous property. Therefore, the recognition of the cells caused the different adhesion process and interfacial viscoelastic properties depending on the surfaces, which were successfully elucidated by the QCM-D techniques.

ASSOCIATED CONTENT

Supporting Information. AFM images of the patterned surface and the cellular pseudopods close to the HAp surface and the height line profiles of the cross section for the broken lines in the images. Δf and ΔD curves of the osteoblast-like cells adhered on PSox and HAp and of the cell adhesion on PSox and HAp without the preadsorption of FBS. CLSM images of the cells adhered on PSox and HAp without the preadsorption of FBS. Fluorescence microscope images of the cells adhered on PSox and HAp. This material is available free of charge via the Internet at http://pubs.acs.org.

AUTHOR INFORMATION

Corresponding Author

*E-mail: tagaya.m.aa@m.titech.ac.jp. Tel: +81-3 5734 3960. Fax: +81-3 5734 3369.

ACKNOWLEDGMENT

M.T. is a research fellow of the Japan Society for the Promotion of Science, Tokyo, Japan.

REFERENCES

(1) Kay, M. I.; Young, R. A.; Posner, A. S. *Nature* **1964**, *204*, 1050–1052.
(2) Kikuchi, M.; Itoh, S.; Ichinose, S.; Shinomiya, K.; Tanaka, J. *Biomaterials* **2001**, *22*, 1705–1711.
(3) Letic-Gavrilovic, L.; Piattelli, A.; Abe, K. *J. Mater. Sci. Mater. Med.* **2003**, *14*, 95–102.
(4) Liao, S. S.; Cui, F. Z. *Tissue Eng.* **2004**, *10*, 73–80.
(5) Yunoki, S.; Ikoma, T.; Monkawa, A.; Ohta, K.; Kikuchi, M,; Sotome, S.; Shinomiya, K.; Tanaka, J. *Mater. Lett.* **2006**, *60*, 999–1002.
(6) Paul, W.; Sharma, C. P. *J. Biomater. Appl.* **2003**, *17*, 253–264.
(7) Kim, H. W.; Knowles, J. C.; Kim, H. E. *J. Biomed. Mater. Res. B* **2005**, *74B*, 686–698.
(8) Mizushima, Y.; Ikoma, T.; Tanaka, J.; Hoshi, K.; Ishihara, T.; Ogawa, Y.; Ueno, A. *J. Controlled Release* **2006**, *110*, 260–265.
(9) Ikoma, T.; Tonegawa, T.; Watanabe, H.; Chen, G. P.; Tanaka, J.; Mizushima, Y. *J. Nanosci. Nanotechnol.* **2007**, *7*, 822–827.
(10) Yongli, C.; Xiufang, Z.; Yandao, G.; Nanming, Z.; Tingying, Z.; Xinqi, S. *J. Colloid Interface Sci.* **1999**, *214*, 38–45.
(11) Ohta, K.; Monma, H.; Takahashi, S, J. *J. Biomed. Mater. Res.* **2001**, *55*, 409–414.

(12) Kandori, K.; Miyagawa, K.; Ishikawa, T. *J. Colloid Interface Sci.* **2004**, *273*, 406–413.
(13) Monkawa, A.; Ikoma, T.; Yunoki, S.; Yoshioka, T.; Tanaka, J.; Chakarov, D.; Kasemo, B. *Biomaterials* **2006**, *27*, 5748–5754.
(14) Yoshioka, T.; lkoma, T; Monkawa, A.; Tonegawa, T.; Chakarov, D; Kasemo, B.; Hanagata, N.; Tanaka, J. *Key Eng. Mater.* **2008**, *361*, 1119–1122.
(15) Ikoma, T; Tagaya, M.; Tonegawa, T.; Takemura, T.; Okuda, M.; Hanagata, N.; Yoshioka, T.; Chakarov, D.; Kasemo, B.; Tanaka, J. *Key Eng. Mater.* **2009**, *396*−*398*, 89–92.
(16) Ikoma, T.; Tagaya, M.; Hanagata, N.; Yoshioka, T.; Chakarov, D.; Kasemo, B.; Tanaka, J. *J. Am. Ceram. Soc.* **2009**, *92*, 1125–1128.
(17) Ikoma, T.; Yamazaki, A.; Nakamura, S.; Akao, M. *J. Solid State Chem.* **1999**, *144*, 272–276.
(18) Tagaya, M.; Ikoma, T.; Takemura, T.; Okuda, M.; Hanagata, N.; Yoshioka, T.; Chakarov, D.; Kasemo, B.; Tanaka, J. *Key Eng. Mater.* **2009**, *396*−*398*, 47–50.
(19) Tagaya, M.; Ikoma, T.; Migita, S.; Okuda., M.; Takemura, T.; Hanagata, N.; Yoshioka, T.; Tanaka, J. *Mater. Sci. Eng. B* **2010**, *173*, 176–181.
(20) Tagaya, M.; Ikoma, T.; Chakarov, D.; Kasemo, B.; Tanaka, J. *Sci. Technol. Adv. Mater.* **2010**, *11*, 045002.
(21) Gurak, E.; Dupont-Gillain, C. C.; Booth, J.; Roberts, C. J.; Rouxhet, P. G. *Langmuir* **2005**, *212*, 10684–10692.
(22) El-Ghannam, A.; Ducheyne, P.; Shapiro, I. M. *J. Orthop. Res.* **1999**, *17*, 340–345.
(23) Rouahi, M.; Champion, E.; Gallet, O.; Jada, A.; Anslme, K. *Colloids Surf., B* **2006**, *47*, 10–19.
(24) Aneslme, K. *Biomaterials* **2000**, *21*, 667–681.
(25) Kasemo, B. *Surf. Sci.* **2002**, *500*, 656–677.
(26) Barrere, F.; Mahmood, T.; Degroot, K.; Vanblitterswijk, C. *Mater. Sci. Eng. R* **2008**, *59*, 38–71.
(27) Nath, N.; Hyun, J.; Ma, H.; Chilkoti, A. *Surf. Sci.* **2004**, *570*, 98–110.
(28) Steele, J. G.; Johnson, G.; Underwood, P. A. *J. Biomed. Mater. Res.* **1992**, *26*, 681–684.
(29) Huang, S. J.; Ingber, D. E. *Exp. Cell. Res.* **2000**, *261*, 91–103.
(30) Webster, T. J.; Siegel, R. W.; Bizios, R. *Biomaterials* **1999**, *20*, 1221–1227.
(31) Okada, S.; Ito, H; Nagai, A.; Komotori, J.; Imai, H. *Acta Biomater.* **2010**, *6*, 591–597.
(32) Nakamura, M.; Nagai, A.; Tanaka, Y.; Sekijima, Y.; Yamashita, K. *J. Biomed. Mater. Res. A* **2009**, *92A*, 783–790.
(33) López-Alvarez, M.; Solla, E. L.; González, P.; Serra, J.; León, B.; Marques, A, P.; Reis, R. L. *J. Mater. Sci. Mater. Med.* **2009**, *20*, 1131–1136.
(34) Hanagata, N.; Takemura, T.; Monkawa, A.; Ikoma, T,; Tanaka, J. *Biochem. Biophys. Res. Commun.* **2006**, *344*, 1234–1240.
(35) Hanagata, N.; Takemura, T.; Monkawa, A.; Ikoma, T.; Tanaka, J. *J. Biomed. Mater. Res. A* **2007**, *83A*, 362–371.
(36) Sauerbrey, G. *Z. Phys.* **1959**, *155*, 206–222.
(37) Nomura, T.; Okuhara, M. *Anal. Chim. Acta* **1982**, *142*, 281–284.
(38) Ebersole, R. C.; Foss, R. P.; Ward, M. D. *Bio-Technology* **1991**, *9*, 450–454.
(39) Gryte, D. M.; Ward, M. D.; Hu, W. S. *Biotechnol. Prog.* **1993**, *9*, 105–108.
(40) Wegener, J.; Janshoff, A.; Galla, H. J. *Eur. Biophys. J.* **1998**, *28*, 26–37.
(41) Elson, J.; Lethem, M. I.; Rees, G. D.; Hunter, A, C. *Biosens. Bioelectron.* **2008**, *23*, 1259–1265.
(42) Muramatsu, H.; Tamiya, E.; Karube, I. *Anal. Chem.* **1988**, *60*, 2142–2146.
(43) Zhou, T.; Marx, K. A.; Warren, M.; Schulze, H.; Braunhut, S. J. *Biotechnol. Prog.* **2000**, *16*, 268–277.
(44) Marx, K. A.; Zhou, T.; Montrone, A.; Schulze, H.; Braunhut, S, J. *Biosens. Bioelectron.* **2001**, *16*, 773–782.
(45) Marx, K. A.; Zhou, T.; Warren, M.; Braunhut, S. J. *Biotechnol. Prog.* **2003**, *19*, 987–999.
(46) Marx, K. A.; Zhou, T.; Montrone, A.; McIntosh, D.; Braunhut, S. J. *Anal. Biochem.* **2005**, *343*, 23–34.
(47) Le Guillou-Buffello, D.; Bareille, R.; Gindre, M.; Sewing, A.; Laugier, P.; Amedee, J. *Tissue Eng. A* **2008**, *14*, 1445–1455.
(48) Fohlerová, Z.; Skládal, P.; Turánek, J. *Biosens. Bioelectron.* **2007**, *22*, 1896–18901.
(49) Wegener, J.; Seebach, J.; Janshoff, A.; Galla, H. J. *Eur. Biophys. J.* **2000**, *78*, 2821–2833.
(50) Janshoff, A.; Wegener, J.; Sieber, M.; Galla, H. J. *Eur. Biophys. J.* **1996**, *25*, 93–103.
(51) Marxer, C. M.; Coen, M. C.; Greber, T.; Greber, U. F.; Schlapbach, L. *Anal. Bioanal. Chem.* **2003**, *377*, 578–586.
(52) Rodahl, M.; Höök, F.; Krozer, A.; Brzezinski, P.; Kasemo, B. *Rev. Sci. Instrum.* **1995**, *66*, 3924–3930.
(53) Rodahl, M.; Höök, F.; Kasemo, B. *Anal. Chem.* **1996**, *68*, 2219–2227.
(54) Höök, F.; Kasemo, B.; Nylander, T.; Fant., C.; Sott, K.; Elwing, H. *Anal. Chem.* **2001**, *73*, 5796–5804.
(55) Rodahl, M.; Kasemo, B. *Rev. Sci. Instrum.* **1996**, *67*, 3238–3241.
(56) Fredriksson, C.; Khilman, S.; Kasemo, B.; Steel, D. M. *J. Mater. Sci.: Mater. Med.* **1998**, *9*, 785–788.
(57) Fredriksson, C.; Khilman, S.; Rodahl, M.; Kasemo, B. *Langmuir* **1998**, *14*, 248–251.
(58) Cans, A.-S.; Höök, F.; Shupliakov, O.; Ewing, A. G.; Eriksson, P. S.; Brodin, L.; Orwar, O. *Anal. Chem.* **2001**, *73*, 5805–5811.
(59) Modin, C.; Stranne, A, L.; Foss, M.; Duch, M; Justesen, J.; Chevallier, J.; Andersen, L, K.; Hemmersam, A. G.; Pedersen, F. S.; Besenbacher, F. *Biomaterials* **2006**, *27*, 1346–1354.
(60) Lord, M.; Modin, C.; Foss, M.; Duch, M.; Simmons, A.; Pedersen, F. S.; Milthorpea, B. K.; Besenbacher, F. *Biomaterials* **2006**, *27*, 4529–4537.
(61) Lord, M. S.; Modin, C.; Foss, M.; Duch, M.; Simmons, A.; Pedersen, F. S.; Besenbacher, F.; Milthorpe, B. K. *Biomaterials* **2008**, *29*, 2581–2587.
(62) Moseke, C.; Ewald, A. *Mater. Wiss Werkstoff.* **2009**, *40*, 36–42.
(63) Voinova, M. V.; Rodahl, M.; Jonson, M.; Kasemo, B. *Phys. Scrip.* **1999**, *59*, 391–396.
(64) Rodahl, M.; Höök, F,; Fredriksson, C.; Keller, C. A.; Krozer, A.; Brzezinski, P.; Voinovaa, M.; Kasemo, B. *Farad. Discuss.* **1997**, *107*, 229–246.
(65) Jenny, M.; Hossein, A.; Peter, K.; Duncan, S. S. *Langmuir* **2007**, *23*, 9760–9768.
(66) Ruoslahti, E.; Pierschbacher, M. D. *Science* **1986**, *233*, 467–470.
(67) Kanazawa, K. K.; Gordon, J, G. *Anal. Chem.* **1985**, *57*, 1770–1771.
(68) Redepenning, J.; Schlesinger, T. K.; Mechalke, E. J.; Puleo, D, A.; Bizios, R. *Anal. Chem.* **1993**, *65*, 3378–3381.
(69) Fernández, P.; Heymann, L.; Ott, A.; Aksel, N.; Pullarkat, P. A. *New J. Phys.* **2007**, *9*, 419–446.
(70) Palmer, A.; Mason, T. G.; Xu, J.; Kuo, S. C.; Wirtz, D. *Biophys. J.* **1999**, *76*, 1063–1071.
(71) Li, F.; Wang, H. C.; Wang, Q. M. *Sens. Actuators, B* **2008**, *128*, 399–406.
(72) Andrew, A. P.; Vladyslav, V. V.; Olga, S. B.; Frederick, W. W. *Eur. Biophys. J.* **1994**, *23*, 197–205.
(73) Heitmann, V.; Reiss, B.; Wegener, J. *Piezoelectric Sensors*; Steinem, C., Janshoff, A., Eds.; Springer Series on Chemical Sensors and Biosensors; Springer: New York, 2007; p 303.